

The September epsilon Perseids in 2013

Štefan Gajdoš¹, Juraj Tóth¹, Leonard Kornoš¹, Jakub Koukal², and Roman Piňff²

An unexpected high activity (outburst) of the meteor shower September epsilon Perseids (SPE) was observed on 2013 September 9/10. The similar event occurred in 2008. We analysed SPE meteors observed in a frame of the European stations network (EDMONd) and collected in the video meteor orbits database EDMOND. Also, we compared two AMOS all-sky video observations of SPE meteors, performed at the Astronomical and Geophysical Observatory in Modra (AGO) and Arborétum in Tesárske Mlyňany (ARBO) stations of the Slovak Video Meteor Network (SVMN). We obtained activity profiles of the 2013 SPE outburst during four hours around its maximum. Along with SPE activity profiles binned at 10 minutes for single-station meteors, we gained orbital characteristics of SPE meteors observed during the outburst, as well as a mean orbits of the SPE meteor stream in interval 2001–2012. The SPE outburst was confirmed by radio forward-scatter observations as well. The obtained observational results might be the starting point for modeling and explanation of SPE outbursts.

Received 2014 March 7

1 Introduction – SPE overview

The September epsilon Perseids meteor shower (SPE, IAU MDC code 208) has a quite long and interesting history. The name was applied for the first time by Denning (1882) who noticed displays of SPE in observations performed on 1869–1880. Hoffmeister (1948) described the SPE by radiant position with coordinates at RA = 53°, DEC = +41°. Drummond (1982) established a new meteor shower – the Delta Aurigids (DAU) active mainly in October – one century after Denning. For a long time, discrepancies were present due to misleading timing of the DAU activity. Recently, Rendtel (1993) searched the IMO database of visual meteors for radiants in area of Perseus and Auriga constellations. He found two separate sources of meteors active in September and October. Rendtel’s analyses clarified the correct periods of activity of the two subsequent meteor showers, also. In the meantime, the SPE were misleadingly attributed as an early appearance of the DAU. The September Perseids are thought active from September 7 to 23 with the maximum on September 12, whilst the DAU are active in the period September 29 – October 18 (Jenniskens, 2006). No source gives ZHR of SPE meteor shower, and no outbursts are mentioned in previous history of September Perseids (Jenniskens, 2006). Besides, SonotaCo (2009) identified September-Perseids meteor shower distinctly through 109 SPE meteors (Table 3 therein), with radiant coordinates as presented in the summary Table 5. Designations as Xi Perseids, September Perseids, September (beta) Perseids and September (epsilon) Perseids are to be found throughout literature.

The SPE were found in the IAU MDC database of precise photographic meteor orbits. Terentjeva (1989) used the name Xi Perseids in her list of 78 bolide meteor showers, for the SPE shower. By using the D-criterion (Southworth & Hawkins, 1963) Porubčan & Gavajdová (1994) found SPE bolides in the IAU MDC

database of 3518 meteor orbits. Ten years later, Gajdoš & Porubčan (2005) found September Perseids meteors in the extended and homogenized database of 4581 orbits.

An outburst of mostly bright September Perseid meteors (SPE) occurred on 2008 September 9. Jenniskens et al. (2008) and other observers (Cooke, 2008; Hergenrother, 2008) reported the outburst with the peak at 8^h20^m ± 20^m UT (solar longitude $\lambda_{\odot} = 166^{\circ}9$). At the Astronomical and Geophysical Observatory (AGO) in Modra, we covered three full nights in the period of 2008 September 6–9. We concentrated on detection, as well as confirmation of a rising activity of the shower. We confirmed that neither outburst nor higher activity of SPE meteors started before 3^h20^m UT, on 2008 September 9, hence we constrained a start of the four-hour-long SPE outburst (Gajdoš et al., 2008). A summary of all above mentioned data along with our new results, presented in this work, are shown in Table 5.

2 Observation of the 2013 outburst of the SPE

In this work, we present an analysis of meteor observations performed by TV/video stations of the European network EDMOND - European viDeo Meteor Observation Network (Kornoš et al., 2013) on 2013 September 9/10. Technical details and operation rules of individual local networks or stations can be found on web-pages of local operators. The EDMOND is a continuously growing network in spread, with coverage from the East to the West Europe. The densest net of TV meteor stations range across the Central-to-South European region. “Extremes” span from UK in the West to the Eastern Ukraine (Figure 1). The EDMOND is operated with various video systems, indeed with individual technical (PC/OS, lenses, detector, intensifier, detection and analysing software, sensitivity, field of view) and observational characteristics. Nonetheless, the observations are comparable and complementary at the same time.

EDMONd network observations with cooperation and data sharing resulted to a creation of the database of meteor orbits EDMOND – European viDeo MeteOr

¹Faculty of Mathematics, Physics and Informatics, Comenius University, Mlynská dolina, 842 48 Bratislava, Slovak Republic

²CEMeNt – Central European Meteor Network

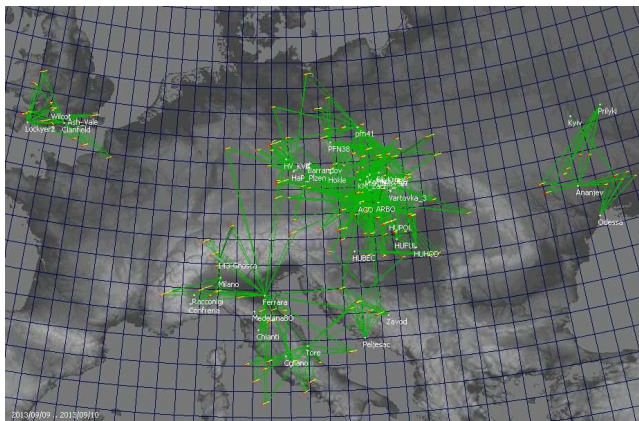


Figure 1 – EDMOND observing sites distribution and multi-station SPE meteors recorded during the night of 2013 September 9/10.

Outburst of sPE'ds on night September 9/10, 2013
690 single September Perseids

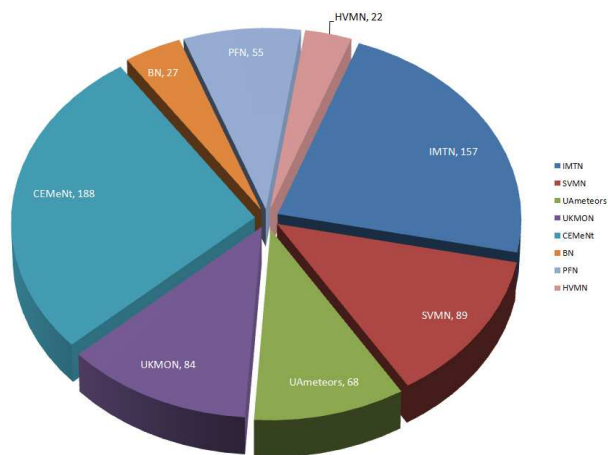


Figure 2 – Total counts of SPE meteors observed by EDMOND stations during the whole night of 2013 September 9/10 – a diagram showing the contribution of local nets.

Database (Kornoš et al., 2014). The database contains more than 1.6 million single-station meteors and 83 369 reliable multi-station meteor orbits. Altogether eight local nets with acceptable weather conditions took part in observations the night 2013 September 9/10. An overview of the EDMOND operation, and counts of observed SPE meteors during the 2013 SPE outburst, is shown in the pie-chart (Figure 2).

2.1 SPE activity profile from all-sky observations

The all-sky observations of the SPE outburst were performed by video systems AMOS at the AGO in Modra and Arborétum in Tesárske Mlyňany (ARBO) on 2013 September 9/10. The system AMOS is described by Zigo et al. (2013) and is able to capture meteors down to visual magnitude +3.5^m. Two stations performed observation over the whole night and we captured the whole display of the SPE outburst.

At the AGO we captured 60 SPE meteors between 21^h UT (on September 9) and 01^h UT (on Septem-

Table 1 – Counts and ratios of SPE meteors recorded at the AGO and ARBO stations, also number of double-station SPE meteors.

Interval of 4-hours on 2013 Sep 9/10	Station AGO	Station ARBO	Double-station SPE meteors
Number of SPEs	60	42	33
Common SPEs ratio	55%	79%	–

ber 10). In the same time span, 42 SPE meteors were recorded at the ARBO station. At both stations, 33 SPE meteors were simultaneously detected (Table 1). Considering negligible interference by clouds, the different counts of detected SPE meteors by one third (the same ratio is valid for overall detected meteors, including non-SPE meteors, for the whole night) can be accounted for instrumental difference and local sky conditions of the two stations. Nevertheless, we tried to find out profiles of SPE activity over four hours around its maximum, for both stations separately, and to compare them.

The numbers of SPE meteors binned in 10 minutes intervals were corrected for radiant elevation for both stations. Other corrections were not applied. Histograms (Figure 3) depict the SPE activity behaviour. The diagrams are apparently the same in profile at both stations, with only small deviations caused by different SPE meteor counts. We tried a binning in shifted intervals (5 or 10 minutes) but no significant differences occur and the resulting histograms are almost identical.

The SPE outburst began suddenly with a steep increase in meteor frequency, with the first display at about 21^h30^m UT. It continued with a broader maximum phase with a first peak at about 22^h05^m UT ±10 minutes, followed by some decrease (gap) of SPE activity, before its next peak at about 22^h40^m UT ±10 minutes. Afterwards, the SPE activity fell to a smooth level, with a frequency similar to the usual SPE maxima in recent years (ZHR 1 to 3 meteors). The broader maximum (with two separated peaks) began and ended with strict “edges”. The main phase ended at the last little peak at about 23^h05^m UT ±10 minutes. According to our records, the maximum (the outburst) lasted no more than two hours.

Single-station SPE radiants for both stations were determined by Gajdoš & Tóth (2013). Here, we only report the mean SPE radiant with coordinates at RA = 47°4 ± 0°1, DEC = +39°5 ± 0°1 for solar longitude λ_☉ = 167°2. Individual values are in Table 5. However, radiants derived from multi-station meteor orbits are more reliable and correct. Thus we calculated radiants of SPE orbits based on EDMOND data. The results are presented in Chapter 2.3.

2.2 SPE 2013 activity profile from EDMOND

All single-station SPE meteors detected by EDMOND from the evening at Ukrainian stations on 2013 September 9 to the morning at UK stations on 2013 September

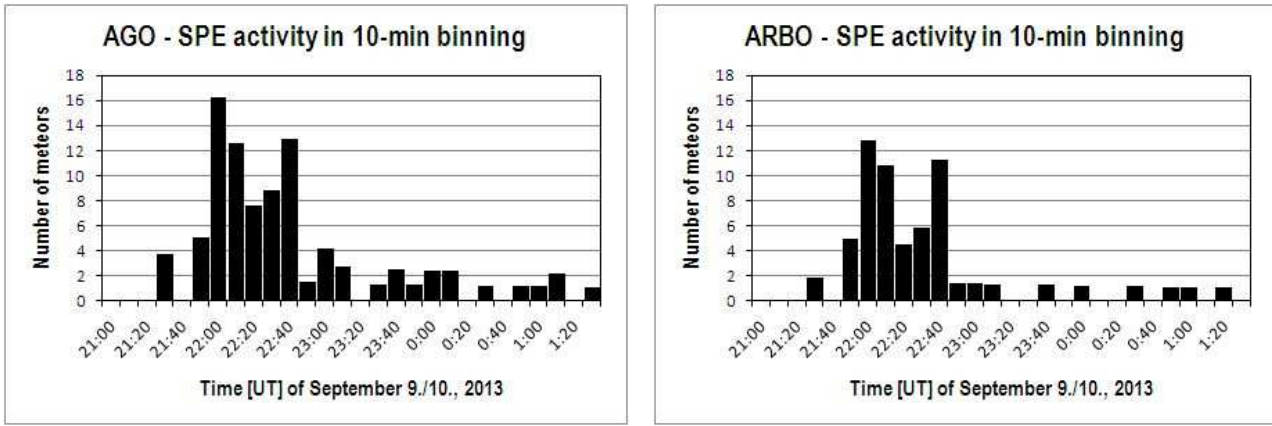


Figure 3 – Number of SPE meteors detected at AGO (left) and ARBO (right) stations binned in 10-min intervals.

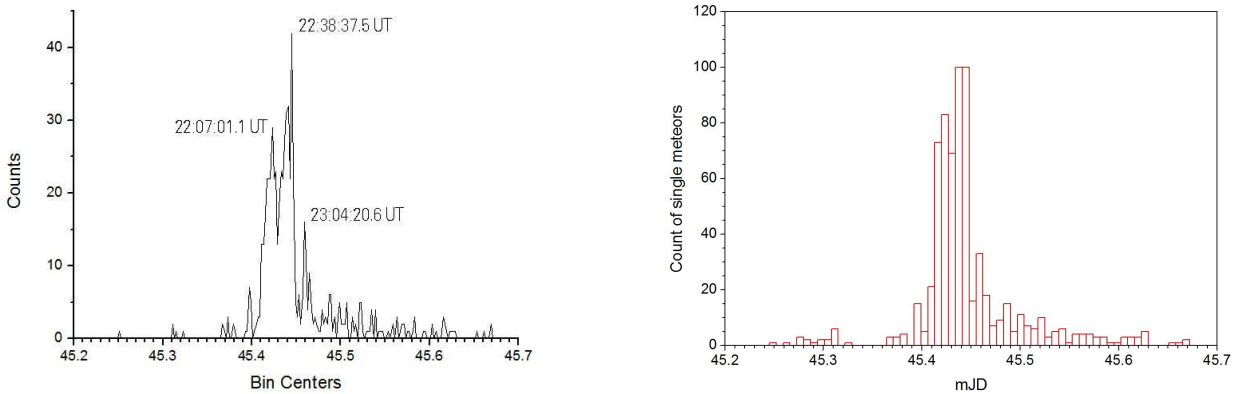


Figure 4 – Counts of EDMOND single-station SPE meteors in smoothed 2-min bins, with three SPE maximum peaks (left), and 10-min bins histogram (right).

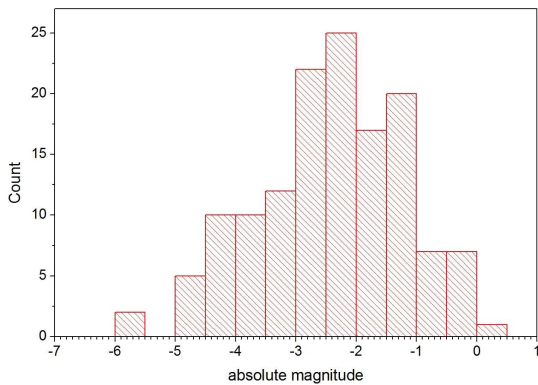


Figure 5 – Absolute magnitude distribution of SPE meteors during outburst 2013.

10, are included in Figure 4, with binning 2 and 10 minutes, respectively. The diagrams reveal a detailed SPE activity over half a day and are consistent with all-sky data.

The only feature which should be resolved in comparison with all-sky data (Figure 3) is a more populated second peak of a broader “plateau” of the maximum. We assume that it simply reflects the number of

video stations in operation across Europe at this time. This could multiply counts of meteors, as one meteor trail can be captured by more stations simultaneously, and so, multiple single-station records of one meteor are present in the EDMOND database (e.g. mid 2012 version contained 11% of multiple records). The situation can be emphasized by presence of brighter meteors which are also detectable (even though at small elevation) at distant stations. This could happen with a prevalence of bigger dust particles (= brighter meteors) in the SPE stream. Such a behaviour with mostly bright meteors was noticed Jenniskens (2008; 2013) in the SPE outburst in 2008, and also after the 2013 outburst. In the EDMOND data we can recognize an occurrence of meteors with visual magnitude mostly in range from $+2^m$ to -4^m during the 2013 SPE outburst, but no dimmer. But the lower visual magnitude value ($+2^m$) is also an instrumental limit for most video stations of the EDMOND network. The absolute magnitude distribution of SPE meteors during the 2013 outburst is shown in Figure 5.

2.3 SPE activity profile from radio forward scatter observations

The single-station (including all-sky) video observations described above gave an activity profile of SPE mete-

Table 2 – Technical parameters and maintenance data of contributing forward-scatter stations.

Name/station	City	State	Location	Antenna	Az	El	Freq.	Receiver	Software
SMRST	Vsetín	CZE	17 °996 E 49 °204 N	X-Beam	80	10	49.75	AOR 8000	HROFFT
E. Stomeo, AAV	Venezia	ITA	12 °374 E 45 °417 N	Yagi 6 el	294	30	143.05	Yaesu FT817	HROFFT
G. de Wilde	Dessel	BEL	5 °100 E 51 °233 N	RHCP	95	45	49.99	SDR	php script
K.-H. Gansel	Dingden	GER	6 °617 E 51 °767 N	T2FD	170	0	143.05	ICOM PCR 1000	php script
I. Sergey	Molodechno	BLR	26 °733 E 54 °267 N	Yagi 5 el	270	0	—	Car radio	MetAn
J. Welkenhuyzen	Lanaken	BEL	5 °627 E 50 °893 N	DIY HB9CV	75	30	49.99	SDR	Speclab

ors during the outburst on 2013 September 9/10 with quite a fine time resolution. We also tend to confirm SPE behaviour detected that night by other kinds of observations. As to visual observation, our (JK from Kroměříž) attempt failed due to local fog at the observing site, thus we have no own information on SPE activity in a visual magnitude range down to +6^m.

Another relevant source of usable data arises from radio forward-scatter observations. We present a diagram of overall meteor activity during 2013 September 9/10, as observed by six stations across the Europe (summary in Table 5). Due to differing instrumental configurations, each of the stations has an individual level of meteor echo counts. We normalized these counts and averaged them to uncover the daily profile of meteor frequency in hourly steps. Figure 6 depicts the averaged meteor hourly rates (solid black line) over one day centered at 2013 September 9.90 UT. The data starting to rise before September 9.85 (20^h24^m) UT and then peaked at about September 9.93 (22^h19^m) UT, which matches video results. Unfortunately, an averaged trend after September 9.95 UT is rather uncertain due to loss of the SMRST station echoes (line with deepest decline; transmitter failure). As the rates presented are not corrected for an observability function, we can only refer to common timing of distinguishable peaks in individual curves. The peak on September 9.95 UT in forward-scatter meteor echoes we account for contribution by enhanced SPE activity.

Coincidence of radio echoes detected by the SMRST station with video counts of SPE video meteors (dark line with a narrow peak) is not evident directly in Figure 7. Corrected hourly rates of meteors detected by SMRST station are depicted by solid line. Vertical lines

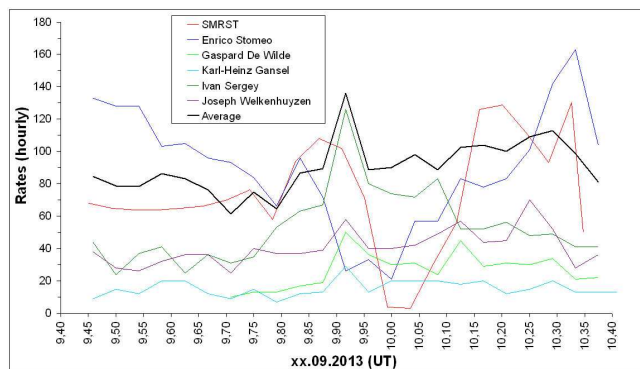


Figure 6 – Forward-scatter observations: averaged hourly rates of echoes on 2013 September 9/10, recorded from six stations across the Europe. Line with deepest decline outlines SMRST station.

denote number of meteor echoes (Y-axis, right) lasting over 10 s and are only indication of incoming SPE outburst. They are in agreement with video observations. The gap in meteor counts after September 9.95 UT is due to transmitter failure and loss of radio signal.

2.4 SPE 2013: meteor orbits and radiants from EDMOND

Based on precise SPE meteor orbits collected in EDMOND, we tried to find out parameters, scale (range) and scattering of SPE stream within a Solar system space. A preview of SPE stream structure is shown in Figure 11.

The video observations within CEMENT and SVMN provided 241 orbits with sufficient quality according to the Kornoš et al. (2014) quality criteria. After the application of radiant ($\pm 5^\circ$) and geocentric velocity ($\pm 10\%$) selection method, 138 SPEs had been identified. As it is clear from Figure 10 (left), the distribution of geocentric velocity V_g is not symmetric as one can expect for very narrow meteor stream. A detailed inspection of video records showed that the spread is caused by uncertainty in velocity determination, mostly due to a small number of measured points along the meteor trail (short angular length and duration of meteor appearance).

To find the core of the stream, the first part of the Welch method (Welch, 2001) with the Southworth-Hawkins D criterion (Southworth & Hawkins, 1963) was applied to the set of 138 SPEs. Using the Welch equa-

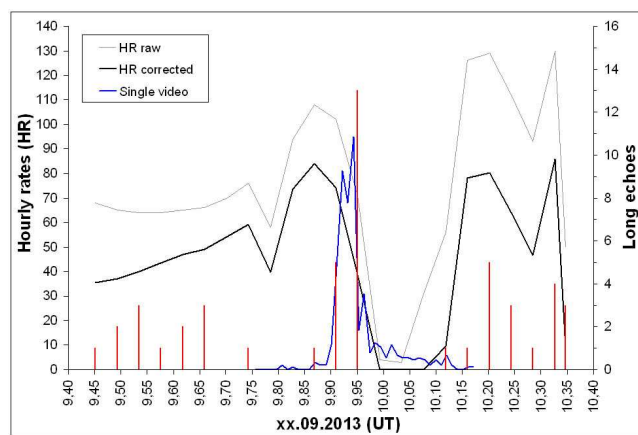


Figure 7 – Radio forward-scatter observation from SMRST station: raw and corrected hourly rates of meteor echoes on 2013 September 9/10. Included are counts of single-station video SPE meteors (dark line with a narrow peak), for comparison. Vertical lines denote number of meteor echoes (Y-axis, right) lasting over 10 s.

tion, the procedure creates a group of meteors around each meteor orbit from the examined shower.

$$\rho_j = \sum_{i=1}^N \left(1 - \frac{D_{ij}^2}{D_c^2} \right) ; \quad D_{ij} \leq D_c . \quad (1)$$

In the Equation (1), ρ_j is a j -th group density at a point in orbital elements space, $N = 138$ is the number of all SPE meteors, D_{ij} is the value obtained for the i -th meteor in the SPE list by comparing its orbit with the orbit which initiates the j -group, and D_c is the threshold value that determines the dynamical similarity among meteor orbits. On the basis of the Equation (1), the value of the density (ρ) is determined for each group and its highest value defines the core of the stream. Satisfying the limiting value $D_c = 0.1$, we have found the core of SPE consisting of 74 meteors. They are presented in Table 3 together with the weighted mean orbit of SPE and standard deviations of all parameters. The comparison of all 138 SPEs (empty columns) with those selected by Welch method (filled columns) is shown in the histograms of the perihelion distance and eccentricity (Figure 8), inclination and argument of perihelion (Figure 9), and geocentric velocity (Figure 10, left), respectively. In the diagram of the radiant position of SPE meteors (Figure 10, right), the core of the stream with higher precision in radiant position is highlighted by black circles, among others (plus signs).

3 Results and discussion

All-sky, single-station video observations, along with radio forward scatter observations gave an activity profile of the SPE during outburst on 2013 September 9/10 with high temporal resolution, and raw overall meteor activity during the night, respectively. We detected distinct peaks, gap and sharp edges in the SPE frequency. We can simply describe the SPE outburst in 2013 as a double-peaked maximum, with three dominant fluctuations (central gap and two edges) during observed interval. Moreover these features are clearly confirmed by both all-sky (Figure 3) and single-station video observations (Figure 4) with very close timing, one notable difference is present. A central gap (in fact a decline of meteor counts) is surrounded by two peaks. But the tops of these peaks differ in level, perhaps depending on the manner of data retrieval. The first peak at 22^h05^m/22^h07^m UT (before the gap) is higher in all-sky systems, while the second peak at 22^h40^m/22^h38^m UT (after the gap) is dominant in histograms based on single-station meteors gathered in EDMOND database. We also identified the third smaller peak at 23^h05^m/23^h04^m UT.

The detected gap as well as the sharp edges in SPE meteor frequency during its outburst are real manifestations of a fine structure of the SPE stream. They could be assigned to two possible reasons: an impossibility of detection of fainter meteors by the video systems used due to their limited instrumental sensitivity, and/or a real absence of smaller particles and thus fluctuations in the mass exponent within a core of the SPE

meteor stream. This could imply the filamentary structure of the stream caused by variation in the flux of dust particles, or variations in population index within the stream. An alternative to the existence of filaments with various size of dust particles is a variable volume density of particles inside the narrow core of the meteoroid stream. Data from visual observation could complete our understanding of the fine structure of the SPE meteor stream.

Mostly brighter meteors were recorded during the SPE outburst in 2013. This could indicate a depletion of smaller dust particles inside the SPE stream. So the Earth crossed a rather older filament mostly occupied by larger particles in the 2013 display. The filament could originate long ago from a parent body, not yet discovered, that would most probably be of the Halley/Thatcher comet type. As to the recurrence of the SPE outbursts, a question arose of the possibility of connecting the events from 2008 and 2013 and making predictions for future.

Acknowledgements

This work was supported by grant APVV-0517-12. We are very grateful to all the forward-scatter observers who provided us with radio data.

References

- Astapovič I. S. and Terentjeva A. K. (1968). “Fireball radiants of the 1st-15th centuries”. In L. Kresák and Millman P. M., editors, *IAU Symp. 33, Tatranská Lomnica, Czechoslovakia, 1967*, Physics and Dynamics of Meteors, Dordrecht. Reidel, pages 308–319.
- Cooke B. (2008). “Fireball outburst”. <http://www.spaceweather.com/archive.php?view=1&day=10&month=09&year=2008> . (10. 9. 2008).
- Denning W. F. (1882). “The September Perseids”. *The Observatory*, **5**, 262–265.
- Drummond J. D. (1982). “A note on the Delta Aurigid meteor stream”. *Icarus*, **51**, 655–659.
- Gajdoš Š. (2005). *Bolide meteor streams*. PhD thesis, Comenius University, Bratislava. (in Slovak).
- Gajdoš Š. and Porubčan V. (2005). “Bolide meteor streams”. In Knežević Z. and Milani A., editors, *Dynamics of Populations of Planetary Systems, IAU Coll. 197, Belgrade 2004*, Cambridge. Cambridge University Press, pages 393–398.
- Gajdoš Š. and Tóth J. (2013). “Septembrové Perzeidy v roku 2013”. *Meteor reports*, **34**, 85–93. (comprehensive abstract in English).
- Gajdoš Š., Tóth J., and Kornoš L. (2008). “Septembrové Perzeidy v roku 2008”. *Meteor reports*, **29**, 44–50. (comprehensive abstract in English).

Table 3 – The core of the September Perseids during outburst on 2013 September 9/10 consisting of 74 orbits. The weighted mean orbit with standard deviations is also presented (λ_{\odot} – solar longitude, RA , DEC – radiant position, V_g – geocentric velocity, q – perihelion distance, e – eccentricity, ω – argument of perihelion, Ω – ascending node, i – inclination, D_{SH} – orbital similarity criterion of meteor orbit). The last two lines are a weighted average, and weighted SD.

λ_{\odot} [°]	RA [°]	DEC [°]	V_g [km/s]	q [AU]	e	ω [°]	Ω [°]	i [°]	D_{SH}	λ_{\odot} [°]	RA [°]	DEC [°]	V_g [km/s]	q [AU]	e	ω [°]	Ω [°]	i [°]	D_{SH}
167.169	47.7	+39.5	63.26	0.703	0.897	248.9	167.2	138.6	0.08	167.202	47.6	+39.8	64.43	0.721	0.972	244.9	167.2	138.7	0.03
167.171	47.9	+39.0	64.13	0.710	0.939	246.9	167.2	139.9	0.03	167.202	47.8	+39.5	63.13	0.701	0.889	249.3	167.2	138.6	0.09
167.172	47.5	+39.0	64.21	0.705	0.952	247.4	167.2	139.8	0.03	167.203	47.1	+39.4	63.24	0.692	0.906	250.0	167.2	138.4	0.09
167.182	48.9	+39.4	64.25	0.730	0.931	244.5	167.2	140.1	0.04	167.204	47.4	+39.4	65.22	0.724	1.022	243.6	167.2	139.5	0.08
167.183	46.6	+39.8	64.64	0.713	1.003	245.4	167.2	138.2	0.05	167.206	47.4	+39.9	62.87	0.699	0.884	249.6	167.2	137.6	0.10
167.185	47.1	+39.0	64.02	0.699	0.948	248.2	167.2	139.3	0.04	167.206	47.0	+39.1	64.17	0.701	0.960	247.7	167.2	139.2	0.03
167.187	46.6	+38.9	64.64	0.699	0.994	247.3	167.2	139.5	0.05	167.206	48.7	+38.8	64.03	0.716	0.916	246.8	167.2	140.8	0.05
167.188	47.5	+39.5	65.30	0.728	1.027	243.0	167.2	139.4	0.09	167.208	47.0	+39.6	64.09	0.707	0.962	246.9	167.2	138.3	0.03
167.188	47.5	+39.4	63.89	0.707	0.938	247.4	167.2	138.9	0.03	167.208	48.0	+39.3	64.09	0.716	0.938	246.3	167.2	139.5	0.02
167.189	47.2	+39.2	64.13	0.703	0.955	247.6	167.2	139.2	0.03	167.208	48.4	+39.2	65.05	0.731	0.989	243.3	167.2	140.5	0.06
167.189	47.5	+40.7	63.99	0.730	0.956	244.1	167.2	137.1	0.05	167.208	48.2	+39.2	64.01	0.715	0.928	246.6	167.2	139.9	0.03
167.190	47.6	+39.3	63.88	0.707	0.933	247.6	167.2	139.2	0.04	167.210	47.8	+39.4	63.39	0.704	0.901	248.6	167.2	138.9	0.07
167.191	47.4	+39.6	63.76	0.708	0.933	247.4	167.2	138.5	0.04	167.210	47.7	+39.4	64.26	0.716	0.955	245.9	167.2	139.3	0.00
167.192	49.5	+40.1	63.74	0.741	0.895	243.8	167.2	139.2	0.07	167.211	47.2	+38.7	65.51	0.715	1.036	244.5	167.2	140.6	0.09
167.192	47.6	+40.4	63.47	0.719	0.920	246.3	167.2	137.3	0.05	167.211	47.3	+39.7	64.48	0.717	0.979	245.3	167.2	138.7	0.03
167.192	47.3	+39.4	65.34	0.725	1.030	243.4	167.2	139.6	0.09	167.211	47.6	+38.3	64.94	0.707	0.988	246.4	167.2	141.2	0.05
167.193	46.5	+39.0	63.52	0.683	0.930	250.6	167.2	138.7	0.09	167.212	47.5	+39.3	63.52	0.701	0.914	248.7	167.2	138.9	0.06
167.194	47.9	+39.6	64.93	0.730	0.997	243.3	167.2	139.4	0.06	167.214	47.0	+39.3	63.83	0.697	0.943	248.5	167.2	138.8	0.05
167.195	46.3	+39.4	64.39	0.698	0.990	247.4	167.2	138.4	0.05	167.214	45.9	+40.1	64.12	0.702	0.990	247.0	167.2	136.8	0.06
167.195	47.4	+39.3	64.60	0.713	0.981	245.7	167.2	139.4	0.03	167.216	47.8	+39.6	65.23	0.731	1.018	242.8	167.2	139.5	0.08
167.195	46.5	+41.0	62.89	0.706	0.912	248.0	167.2	135.4	0.09	167.216	48.3	+39.4	64.88	0.731	0.984	247.9	167.2	138.5	0.04
167.195	48.7	+39.3	64.31	0.728	0.937	244.8	167.2	140.2	0.03	167.217	47.8	+39.3	64.29	0.715	0.956	246.0	167.2	139.4	0.00
167.195	47.2	+39.4	65.18	0.722	1.023	243.9	167.2	139.4	0.08	167.218	47.3	+40.3	64.63	0.728	0.997	243.6	167.2	137.8	0.06
167.195	47.6	+39.5	63.01	0.698	0.884	249.8	167.2	138.4	0.10	167.218	48.1	+40.1	64.06	0.728	0.943	244.6	167.2	138.4	0.03
167.195	47.2	+40.9	64.36	0.734	0.988	242.9	167.2	136.7	0.08	167.224	47.4	+37.5	64.73	0.688	0.972	249.1	167.2	142.2	0.08
167.196	48.2	+39.5	65.30	0.737	1.014	242.2	167.2	139.9	0.09	167.228	46.8	+38.9	64.99	0.706	1.013	246.1	167.2	139.8	0.06
167.196	47.9	+39.0	64.79	0.720	0.980	244.9	167.2	140.2	0.04	167.229	47.9	+39.5	63.71	0.710	0.919	247.4	167.2	139.0	0.04
167.196	48.0	+39.0	64.59	0.717	0.966	245.6	167.2	140.3	0.02	167.230	48.1	+38.7	65.09	0.721	0.993	244.6	167.2	141.0	0.05
167.197	49.5	+38.9	64.59	0.737	0.935	243.6	167.2	141.4	0.06	167.231	47.3	+39.1	63.44	0.693	0.912	249.7	167.2	139.0	0.08
167.198	47.7	+40.6	64.86	0.742	1.009	241.6	167.2	137.7	0.10	167.233	47.4	+40.2	64.27	0.723	0.972	244.7	167.2	137.9	0.04
167.198	47.7	+39.6	65.15	0.730	1.014	243.1	167.2	139.4	0.08	167.235	50.5	+39.8	63.93	0.752	0.884	242.6	167.2	140.4	0.10
167.198	46.9	+39.4	63.97	0.702	0.954	247.7	167.2	138.5	0.04	167.236	48.2	+39.0	65.13	0.727	0.998	243.7	167.2	140.5	0.06
167.199	47.6	+39.3	64.09	0.710	0.945	246.9	167.2	139.3	0.02	167.238	46.2	+40.7	63.35	0.703	0.944	247.8	167.2	135.8	0.07
167.201	46.9	+39.7	64.49	0.713	0.988	245.6	167.2	138.4	0.04	167.244	46.0	+39.4	64.65	0.699	1.014	246.9	167.2	138.2	0.07
167.201	48.8	+39.4	64.92	0.739	0.975	242.5	167.2	140.3	0.07	167.267	47.2	+39.3	64.02	0.703	0.952	247.6	167.3	138.8	0.03
167.201	48.1	+39.2	63.25	0.702	0.886	249.2	167.2	139.3	0.09	167.271	48.8	+39.4	65.20	0.740	0.995	242.0	167.3	140.4	0.08
										167.284	47.0	+39.4	63.79	0.699	0.943	248.3	167.3	138.4	0.05
										167.206	47.6	+39.4	64.27	0.714	0.959	246.1	167.2	139.1	0.04
										0.02	0.7	0.5	0.52	0.012	0.032	1.8	0.0	1.1	0.02

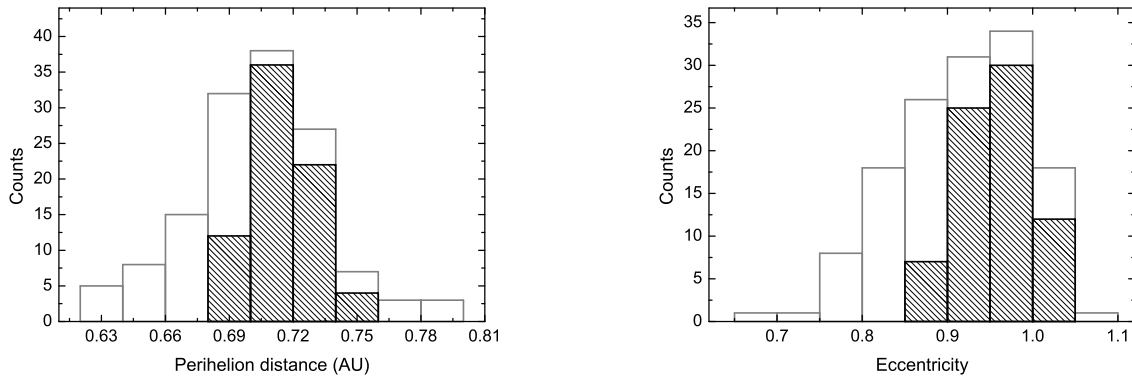


Figure 8 – Histogram of SPE meteors perihelion distances (left) and eccentricities (right). Empty columns depict all SPE orbits, whereas filled ones depict the SPE core.

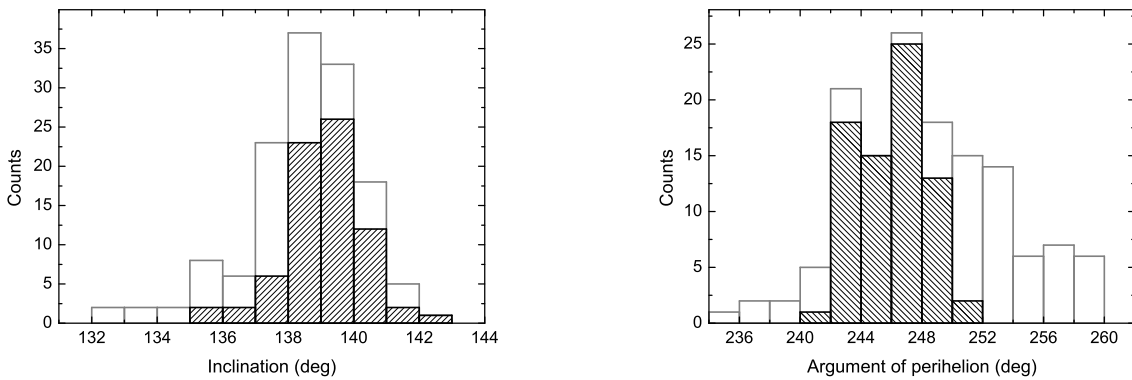


Figure 9 – Histogram of SPE meteors inclination (left) and argument of perihelion (right). Empty columns depict all SPE orbits, whereas filled ones depict the SPE core.

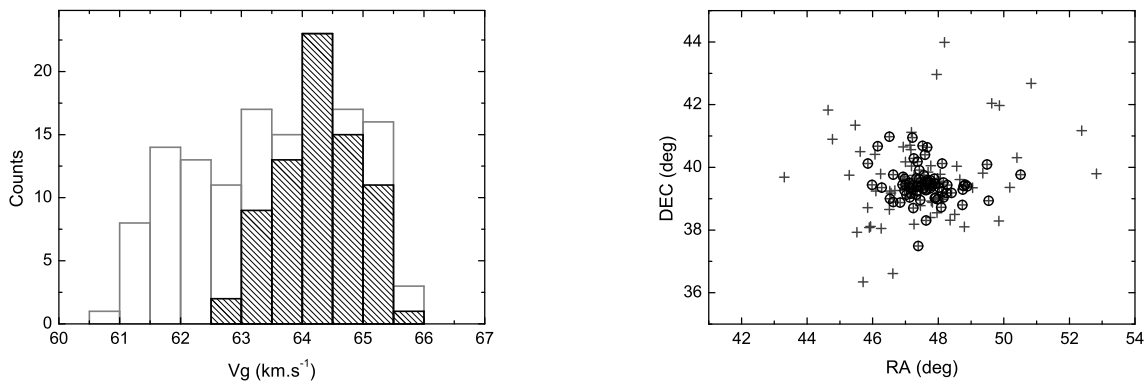


Figure 10 – Histogram of SPE meteors geocentric velocities (left) and diagram of SPE radiants (right). Empty columns depict all SPEs, whereas filled ones depict the SPE core. The core of the stream with higher precision in radiant position is highlighted by black circles, among others (plus signs).

Gavajdová M. (1994). “On the population of very bright meteors in meteor streams”. *Contrib. Astron. Obs. Skalnaté Pleso*, **24**, 101–110.

Hergenrother C. (2008). “Sept 8/9 meteors”. <http://transientsky.wordpress.com/2009/09/09/sept-89-meteors/>. (9. 9. 2008).

Hoffmeister C. (1948). *Meteorströme*. J. A. Barth, Leipzig, 79-93 pages.

Jenniskens P. (2006). *Meteor Showers and Their Parent Comets*. Cambridge Univ. Press, Cambridge, U.S.A.

Jenniskens P. (2013). “September epsilon Perseids 2013”. *CBET*, **3652**.

Jenniskens P., Brower J., Martsching P., Lyytinen E., Entwistle D., and Cooke W. J. (2008). “September Perseid Meteors 2008”. *CBET*, **1501**.

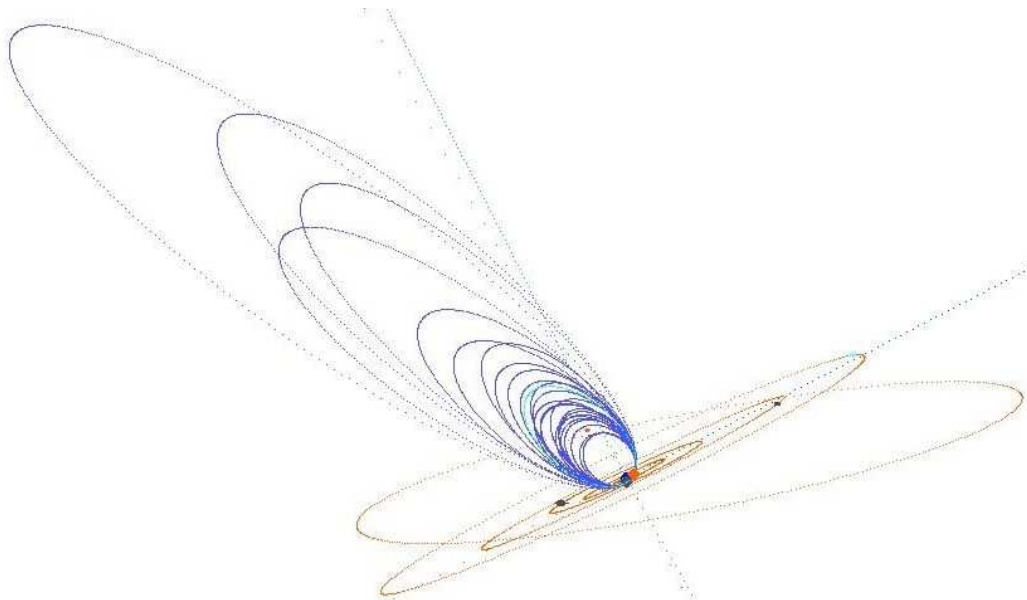


Figure 11 – Orientation and form of the SPE meteor stream – orbits in 2013.

Table 4 – A comparison of the SPE orbits: from IAU MDC, orbit from EDMOND for 2001–2012, averaged orbit from EDMOND for 2007–2012, and mean orbit for outburst 2013 (Year/Source, RA , DEC – radiant position, V_g – geocentric velocity, q – perihelion distance, e – eccentricity, ω – argument of perihelia, Ω – ascending node, i – inclination, a – semimajor axis).

Method	RA [°]	DEC [°]	V_g [km/s]	q [AU]	e	ω [°]	Ω [°]	i [°]	a [AU]	D_{SH}
IAU MDC	50.2	+39.4	64.5	0.742	—	241.9	171.3	138.9	31.1	—
2001–2012	47.2	+39.5	63.8	0.709	0.931	247.3	166.9	138.7	10.3	0.03
SD	2.2	0.6	0.42	0.016	0.034	2.2	1.9	0.9	—	0.01
2007–2012	47.9	+39.3	63.5	0.707	0.919	247.9	166.9	139.0	8.8	—
SD	5.5	1.7	2.52	0.090	0.134	13.5	0.1	3.9	—	—
SPE 2013	47.6	+39.4	64.3	0.714	0.959	246.1	167.2	139.1	17.4	0.04
SD	0.7	0.5	0.52	0.012	0.032	1.8	0.0	1.1	—	0.02

Kornoš L., Koukal J., Piff R., and Tóth J. (2013). “Database of meteoroid orbits from several European video networks”. In Gyssens M. and Roggemans P., editors, *Proceedings of the IMC 2012*. IMO, pages 21–25.

Kornoš L., Koukal J., Piff R., and Tóth J. (2014). “EDMOND meteor database”. In Gyssens M., Roggemans P., and Žołądek P., editors, *Proceedings of the International Meteor Conference, Poznań, Poland, Aug. 22-25, 2013*. International Meteor Organization. (submitted).

Porubčan V. and Gavajdová M. (1994). “A search for fireball streams among photographic meteors”. *Planet. Space Sci.*, **42**, 151–155.

Rendtel J. (1993). “Delta Aurigids and September Perseids”. In Štohl J. and Williams I., editors, *Meteoroids and their parent bodies*. Astronomical Inst., Slovak Acad. Sci., Bratislava, pages 185–188.

Rendtel J. and Arlt R., editors (2008). *Handbook for meteor observers*. IMO, Potsdam.

Rendtel J. and Molau S. (2010). “Meteor activity from

the Perseus-Auriga region in September and October”. *WGN, Journal of the IMO*, **38:5**, 161–166.

SonotaCo (2009). “A meteor shower catalog based on video observations in 2007–2008”. *WGN, Journal of the IMO*, **37:2**, 55–62.

Southworth R. and Hawkins G. (1963). “Statistics of meteor streams”. *Smithson. Contr. Astrophys.*, **7**, 261–285.

Terentjeva A. K. (1989). “Fireball streams”. *WGN, Journal of the IMO*, **17**, 242–245.

Welch P. G. (2001). “A new search for streams in meteor data bases and its application”. *MNRAS*, **328**, 101–111.

Zigo P., Tóth J., and Kalmančok D. (2013). “All-sky Meteor Orbit System (AMOS)”. In Gyssens M. and Roggemans P., editors, *Proceedings of the IMC 2012*. IMO, pages 18–20.

Handling Editor: Javor Kac

This paper has been typeset from a \LaTeX file prepared by the authors.

Table 5 – Summary of available sources on SPE and incidental meteor showers: solar longitude λ_{\odot} (in degrees), radiant coordinates (right ascension, declination, in degrees) and geocentric velocity V_g in km/s).

Source	λ_{\odot}	RA	DEC	V_g
W. F. Denning (1882)	—	61.5	+36.2	—
C. Hoffmeister (1948)	—	53	+41	—
I. S. Astapovič & A. K. Terentjeva (1968)	—	54.8	+36.2	—
J. D. Drummond (1982, Delta Aurigids)	—	83.5	+50.4	64.9
A. K. Terentjeva (1989)	—	54.8	+36.2	67.1
J. Rendtel (1993)	—	51.5	+39.5	65.6
V. Porubčan & M. Gavajdová (1994)	—	47.2	+38.9	65.4
M. Gavajdová (1994, $\leq -9^m$)	—	47.2	+39.5	64.9
P. G. Welch (2001)	165.6	48.3	+39.1	—
Š. Gajdoš & V. Porubčan (2005)	—	47.4	+39.0	65.6
Š. Gajdoš (2005)	—	51.0	+38.8	65.7
P. Jenniskens (2006)	170.0	50.2	+39.4	64.5
SonotaCo (2009)	167.1	47.3	+39.3	63.9
J. Rendtel & R. Arlt (2008), IMO Handbook	166.7	60	+47	64
B. Cooke (2008)	166.9	49.5	+43.0	—
C. Hergenrother (2008)	166.9	49	+39	—
Š. Gajdoš, J. Tóth, L. Kornoš (2008)	166.6	47.4	+39.7	—
Š. Gajdoš & J. Tóth (2013), for AGO	167.2	47.5	+39.4	—
Š. Gajdoš & J. Tóth (2013), for ARBO	167.2	47.3	+39.6	—
This work	167.2	47.6	+39.4	64.3